Mineralogical Magazine, October 2008, Vol. 72(5), pp. 999–1010

Mushroom elbaite from the Kat Chay mine, Momeik, near Mogok, Myanmar: II. Zoning and crystal growth

A. J. Lussier[1], F. C. Hawthorne[1,*], S. Herwig[1], Y. Abdu[1], P. M. Aguiar[2], V. K. Michaelis[2] and S. Kroeker[2]

[1] Department of Geological Sciences, University of Manitoba, Winnipeg, Manitoba, Canada R3T 2N2
[2] Department of Chemistry, University of Manitoba, Winnipeg, Manitoba, Canada R3T 2N2

[*Received 4 December 2008; Accepted 10 December 2008*]

ABSTRACT

A variety of mushroom tourmaline from the Kat Chay mine, Momeik, near Mogok, Shan state, Myanmar, consists of a black-to-grey single-crystal core from which a single prismatic crystal reaches to the edge of the mushroom, forming a slight protuberance. The rest of the mushroom (~50% by volume) consists of extremely acicular sub-parallel crystals that diverge toward the edge of the mushroom. The acicular crystals are dominantly colourless to white, with a continuous black zone (2 mm across) near the edge, and pale pink outside the black zone. The composition varies from ~$Na_{0.75}Ca_{0.05}(Li_{0.80}Al_{0.70}Fe_{1.10}Mn_{0.30}Ti_{0.10})Al_6Si_6(BO_3)_3O_{18}(OH)_3(OH,F)$ at the base of the mushroom to ~$Na_{0.60}Ca_{0.06}(Li_{1.00}Al_{1.98}Fe_{0.02})Al_6(Si_{5.35}B_{0.65})(BO_3)_3O_{18}(OH)_3(OH,F)$ close to the edge at the top of the mushroom. The principal substitutions are: (1) $^{Y}Li + {}^{Y}Al \rightarrow {}^{Y}Fe^* + {}^{Y}Fe^*$ and (2) $^{T}B + {}^{Y}Al \rightarrow Si + {}^{Y}Fe^*$, but there are five other minor substitutions that are also operative. There are six significant compositional discontinuities at textural boundaries in the mushroom, suggesting that the changes in habit are driven in part by changes in external variables such as *T* and *P*, plus possible involvement of new fluid phases.

Keywords: elbaite, tourmaline, electron microprobe analysis, zoning, Mogok, Myanmar.

Introduction

Tourmaline from the granitic pegmatites in the region of Momeik, northeast of Mogok and northwest of Sakangyi, show unusual mushroom-like habits. Lussier *et al.*, 2008 described the crystal chemistry of two samples of mushroom tourmaline from the Kat Chay mine, Momeik, Mandalay Division, Myanmar. They used ^{11}B and ^{27}Al Magic Angle Spinning Nuclear Magnetic Resonance spectroscopy (MAS NMR) to show the presence of ^{iv}B and the absence of ^{iv}Al in samples with transition metals low enough to prevent paramagnetic quenching of the signal. There has been considerable work on the substitution of B for Si in tourmalines, both by MAS NMR (Tagg *et al.*, 1999; Schreyer *et al.*, 2000; Marler and Ertl, 2002; Lussier *et al.*, 2008, 2009) and crystal-structure refinement (Ertl *et al.*, 1997; Hughes *et al.*, 2000, 2004; Hughes, 2001; Kalt *et al.,* 2001; Marler *et al.*, 2002; Ertl *et al.*, 2005, 2006, 2007; Lussier *et al.*, 2008, 2009) from granitic pegmatites, and it is now well established that the *T*-site in tourmaline can accommodate considerable ^{iv}B (up to 1 a.p.f.u.). Similarly, both ^{27}Al MAS NMR (Lussier *et al.*, 2008, 2009) and crystal-structure refinement (MacDonald and Hawthorne, 1995; Bloodaxe *et al.*, 1999; Schreyer *et al.*, 2002; Cempírek *et al.*, 2006; Prowatke *et al.*, 2003; Ertl and Hughes, 2002; Ertl *et al.*, 2003) have shown significant substitution of Al for Si at the *T* site in tourmaline.

Well developed compositional zonation in elbaitic tourmalines often reflects growth in pockets in a miarolitic pegmatite (e.g. London and Manning, 1995; Federico *et al.*, 1998; London, 1999; Selway *et al.*, 1999, 2000, 2002; Dutrow and Henry, 2000) and, as such, can record

* E-mail: frank_hawthorne@umanitoba.ca
DOI: 10.1180/minmag.2008.072.5.999

the evolution of hydrothermal fluids (Dutrow and Henry, 2000). Mushroom tourmaline from Momeik may show prominent changes in colour, indicating changes in composition that correlate strongly with habit. Here, we examine the compositional zoning associated with the unusual habit in mushroom tourmaline from Momeik.

Mushroom tourmaline: habit

Sample SHM (Fig. 1) consists of a base of black, dense tourmaline that grades into a greyish-white aggregate of parallel acicular crystals, reverting to a thin band of black acicular tourmaline that is mantled by a thick cap of pink tourmaline. In this and subsequent figures, the samples are oriented with the *c* axes of the constituent crystals approximately vertical.

A thick section through the centre of the mushroom shows that the pink-coloured material that appears dominant in Fig. 1 is actually a pink rind over a more extensive white, grey and black core (Fig. 2*a*). Transmitted light shows the presence of three morphologically distinct regions. The base is an optically continuous single crystal that changes colour from black to pink to grey in the *c* direction. In the centre of the sample, a prismatic optically continuous crystal extends from the centre of the base in the *c* direction; this crystal is ~3 cm long and 0.3 cm across, and is optically continuous with the core itself. Where this crystal approaches the black zone of the rind, it divides into numerous acicular crystals (Fig. 3*a*) that diverge, broadening the central crystal at the top of the sample, making a small protrusion at the apex of the sample and a discontinuity in the peripheral black zone. On either side of the long prismatic crystal, the core crystal splits into numerous acicular crystals (Figs 2*b*, 3*b*), imparting a splintery texture to this part of the sample. At the base of the prismatic crystal, the *c* axes of the acicular crystals are parallel to the *c* axis of the central prismatic crystal (Fig. 3*b*), but further along the prismatic crystal, the acicular crystals diverge from the central prismatic crystal (Fig. 3*c*). The acicular crystals pass through the black and pink parts of the sample and impart an irregular rounded aspect to the surface, somewhat resembling the surface of a cauliflower. In the outer part of the rind, the acicular crystals can interweave, giving a very mottled appearance in cross-polarized light. A thick section orthogonal to the *c* direction (Fig. 2*c*–*e*) shows the central prismatic crystal surrounded by microcrystals (cross-sections of acicular crystals). The central prismatic crystal is rather irregular in outline (only half the cross-section is visible, and is best seen in Fig. 2*e*), rather than triangular or hexagonal. Overall, the sample has the appearance of a mushroom.

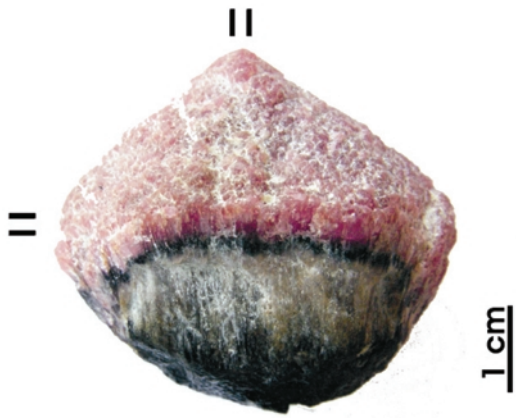

FIG. 1. Pink-white-black Mogok mushroom tourmaline (SHM); (||) and (=) mark the approximate location and thickness of the polished sections shown in Fig. 2*c*–*e*.

Electron microprobe analysis

Electron microprobe data were collected on a polished slab of SHM (Fig. 2*b*) using a Cameca SX100 electron microprobe operating at 15 kV, probe current 20 nA, beam diameter 10 μm, peak count-time 20 s, background count-time 10 s, using the standards described by Lussier *et al.*, 2008. ^{11}B and ^{27}Al MAS NMR spectra (Lussier *et al.*, 2009) showed that the *T* site is occupied only by Si and B, and hence the formulae were normalized on 31 anions with [OH + F] = 4 a.p.f.u., Si + B = 9 a.p.f.u., and Li = 15 − Σ (*Y* + *Z* + *T*) a.p.f.u. The question now arises as to the accuracy of the calculation for ^{iv}B. In general, such a calculation cannot be justified without spectroscopic evidence that ^{iv}Al does not occur. Where this is the case, ^{iv}B is determined by the value of Si in a.p.f.u., and hence the error associated with ^{iv}B is the same as that associated with Si. Examination of the total range of SiO_2 values for ten points on homogeneous tourmaline crystals gives an average range of ~0.40 wt.% oxide. Using this range of SiO_2 values in the calculation of a tourmaline formula gives a range

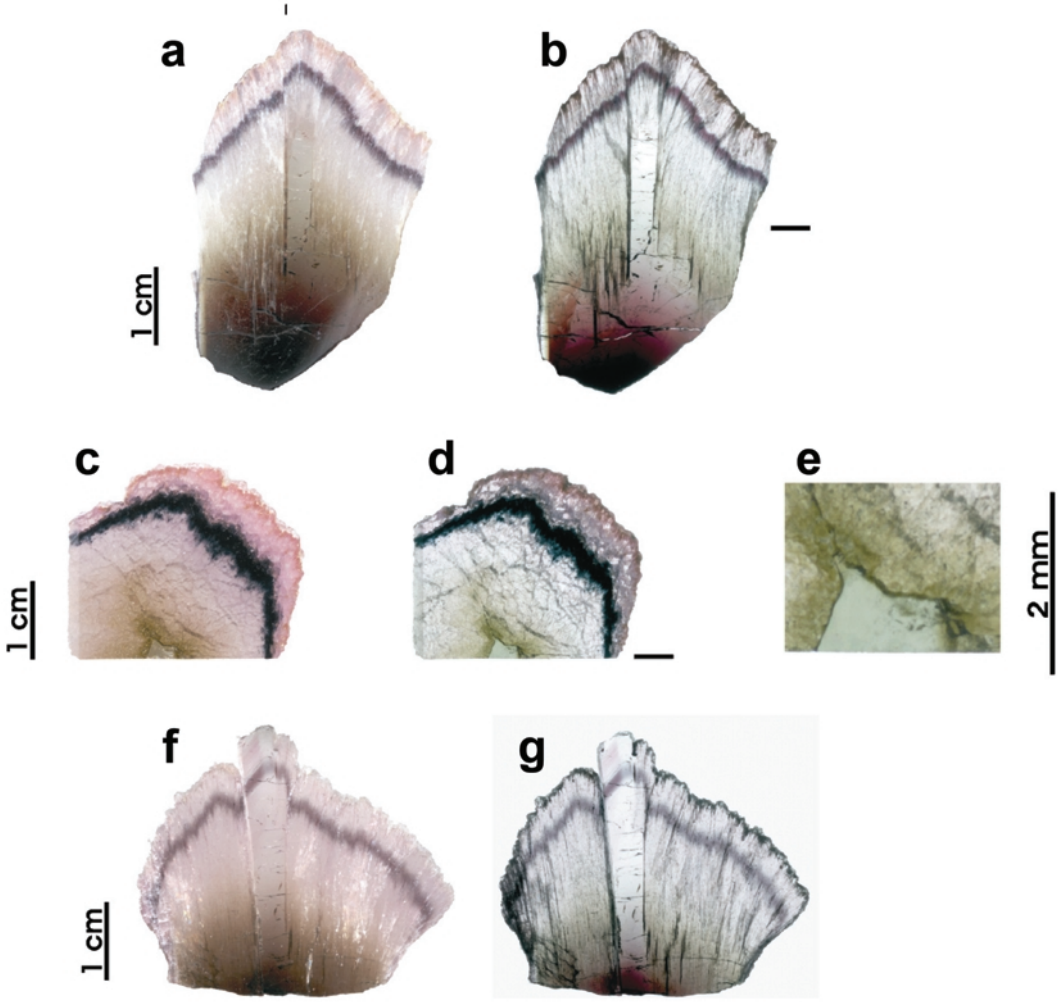

FIG. 2. Doubly-polished sections (~1 mm thick) of the mushroom tourmalines in both reflected (*a*, *c*, *f*) and transmitted (*b*, *d*, *e*, *g*) light; (*a*, *b*) SHM cut parallel to the *c* axis; (*c*, *d*, *e*) SHM cut orthogonal to *c* axis; (*e*) is an enlargement of the central prismatic crystal; (*f*, *g*) SHP cut parallel to the *c* axis. Note, the symbol – in (*b*) and (*d*) denotes the line of intersection of the two SHM sections.

in Si (a.p.f.u.) values of ~0.04 a.p.f.u., which is thus a measure of the uncertainty associated with the ^{iv}B values given here. Note that this applies only where spectroscopic work has shown that ^{iv}B is present and ^{iv}Al is absent.

Chemical variation in mushroom tourmaline

Figure 4 shows the analytical traverses across mushroom tourmaline SHM. Figure 5 summarizes the variation in cations as a function of position along a traverse (Fig. 4) across the black core at the base of the crystal (points 1–10), the central prismatic crystal (points 11–36), the black zone (point 37), and the pink rim (points 38–45). The sum of the transition metals is ~1.30 a.p.f.u. at the base of the core (Fig. 5*a*), falls rapidly to ~0.50 a.p.f.u. at the junction between the core and the central prismatic crystal, then decreases more slowly with distance along the crystal, gradually approaching 0.00 a.p.f.u. at the edge of the pink rim. The narrow black zone that is a very prominent feature of this sample (Figs 1,2) shows a sharp rise in total transition

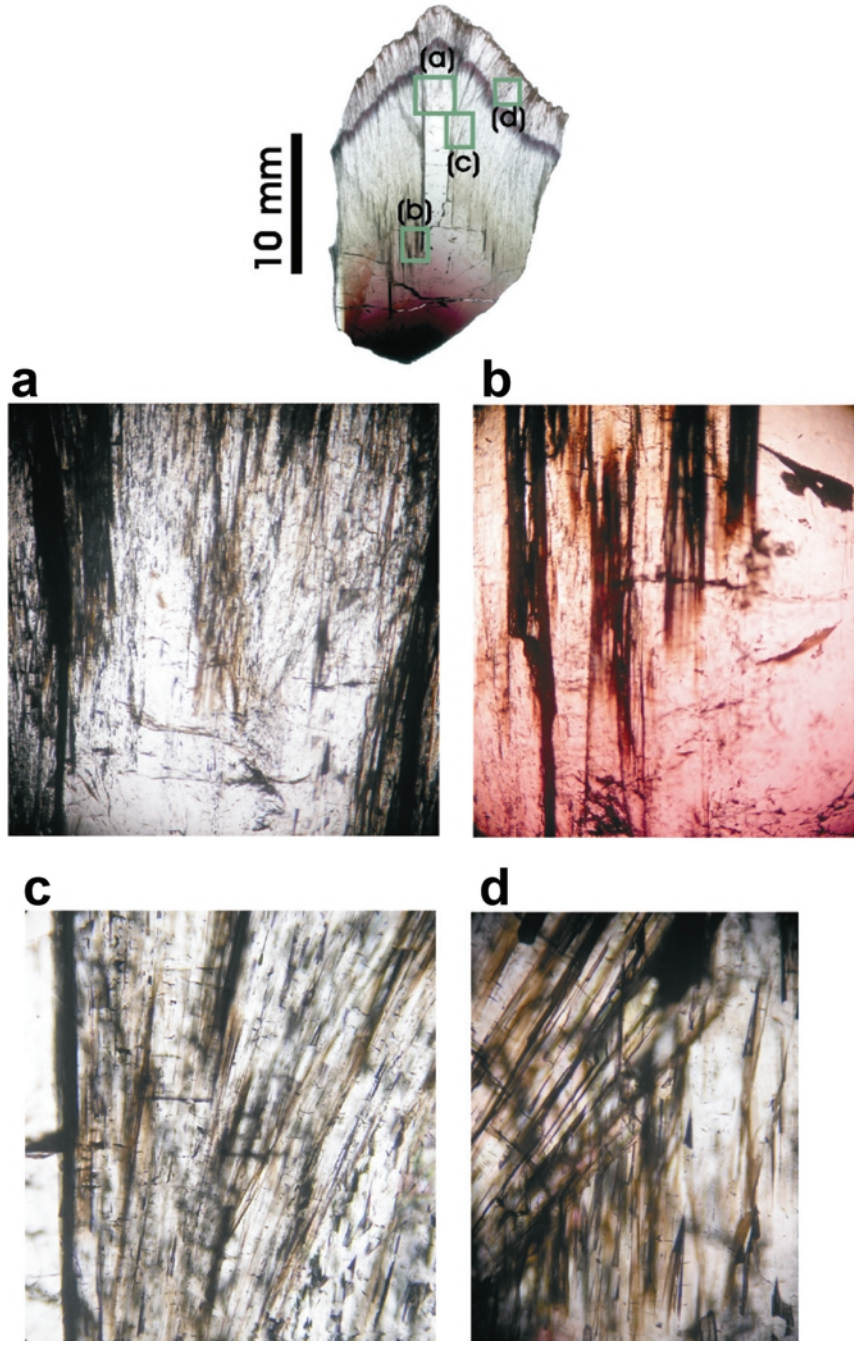

FIG. 3. High-magnification photographs of SHM in plane-polarized light, showing the character of the grain boundaries: (*a*) transition of the central prismatic crystal to numerous acicular crystals; (*b*) transition of the core region from a single crystal to numerous acicular crystals; (*c*) the divergence of acicular crystals from the central prismatic crystal visible at the extreme left of the photograph; (*d*) interpenetration of acicular crystals of different orientation.

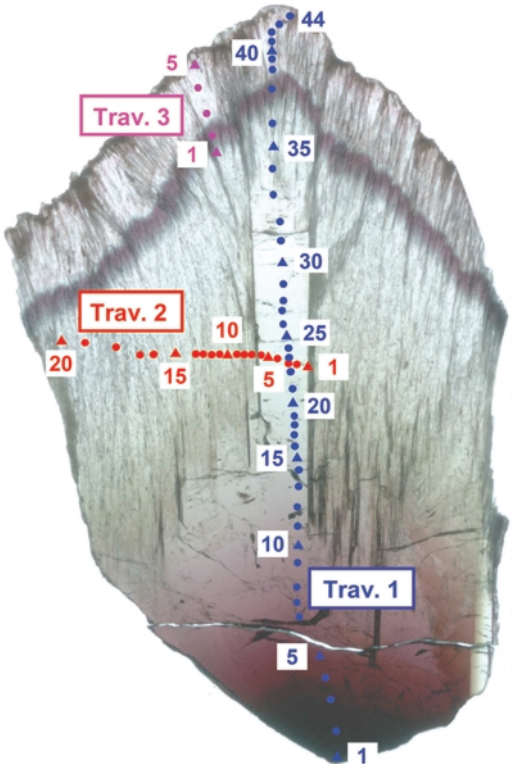

FIG. 4. Section of SHM showing the traverses and the positions of the analytical points illustrated in Figs 5–9.

metals. Individual transition metals follow a similar trend (Fig. 5*a*), except that the Fe content falls below the Mn content halfway along the central prismatic crystal, only to increase strongly in the black zone (where the Mn content does not increase at all). Both Li and ^{Y}Al increase strongly from the base to the edge of the core; the Li content flattens out along the length of the central prismatic crystal, whereas ^{Y}Al continues to increase. At the boundary between the core and the base of the prismatic crystal, there are small but distinct discontinuities in Li and ^{Y}Al (Fig. 5*b*). There are also discontinuities at the black zone, the contents of both Li and ^{Y}Al dropping by 0.10–0.20 a.p.f.u. In the pink rim, the variation of Li and ^{Y}Al becomes more irregular.

The variation in Na at the *X* site also shows strong discontinuities at the boundary between the core and the base of the prismatic crystal, and at the black zone (Fig. 5*c*). Na decreases strongly through the black core, decreases less strongly along the central prismatic crystal, increases strongly in the black zone, and then decreases strongly in the pink rim. The calculated ^{iv}B increases continuously from the base of the core to the boundary with the central prismatic crystal where there is a jump in ^{iv}B, followed by a steady increase along the length of the central crystal. In the pink rim, the variation in ^{iv}B at first seems very irregular, but in fact shows a strong correlation with the variation in ^{Y}Al and Li (see below).

Substitution mechanisms in mushroom tourmaline

Figure 5 indicates a major discontinuity in chemical variation at the boundary between the core and the base of the prismatic crystal, and another major discontinuity at the black zone close to the margin of the sample. Figure 6 shows the variation in cations as a function of Fe* content (Fe* = Fe + Mn + Ti) in the black core and the prismatic crystal. In the black core (Fig. 6*a*), all cations show linear variation as a function of Fe* content, and we may use these variations to identify the major substitutions from the possible cation exchanges that can occur, together with the amounts of these substitutions (indicated by the numbers after the exchanges). For the black core, these substitutions are given below:

(1) ^{Y}Li + ^{Y}Al → ^{Y}Fe* + ^{Y}Fe* 0.25 a.p.f.u.
(2) ^{T}B + ^{Y}Al → Si + ^{Y}Fe* 0.15 a.p.f.u.
(3) $^{X}\square$ + ^{Y}Al → Na + ^{Y}Fe* 0.09 a.p.f.u.
(4) ^{Y}Al → ^{Y}Fe^{3+} 0.09 a.p.f.u.

The straight lines in Fig. 6*a* show the aggregate variations represented by these substitutions.

The same variations are shown for the central prismatic crystal in Fig. 6*b*. As is apparent in Fig. 5*a*, there is a slight discontinuity halfway along the crystal, where the slopes of the variations in ^{Y}Al and ^{iv}B increase (by the same amount) and the slopes of the variations in Li and Na decrease (again by approximately the same amount) (Fig. 6*b*). In the first half of the crystal, the following changes occur: ^{Y}Al (+0.11), Li (+0.05), Fe* (−0.15), B (−0.06) and Ca (−0.04 a.p.f.u.); thus Li and ^{Y}Al continue to increase and Fe* decreases, and hence substitution (1) continues, increasing Li and ^{Y}Al by 0.06 a.p.f.u. and decreasing Fe* by 0.12 a.p.f.u.. The remaining changes relate to substitution (5) below, and thus the compositional changes

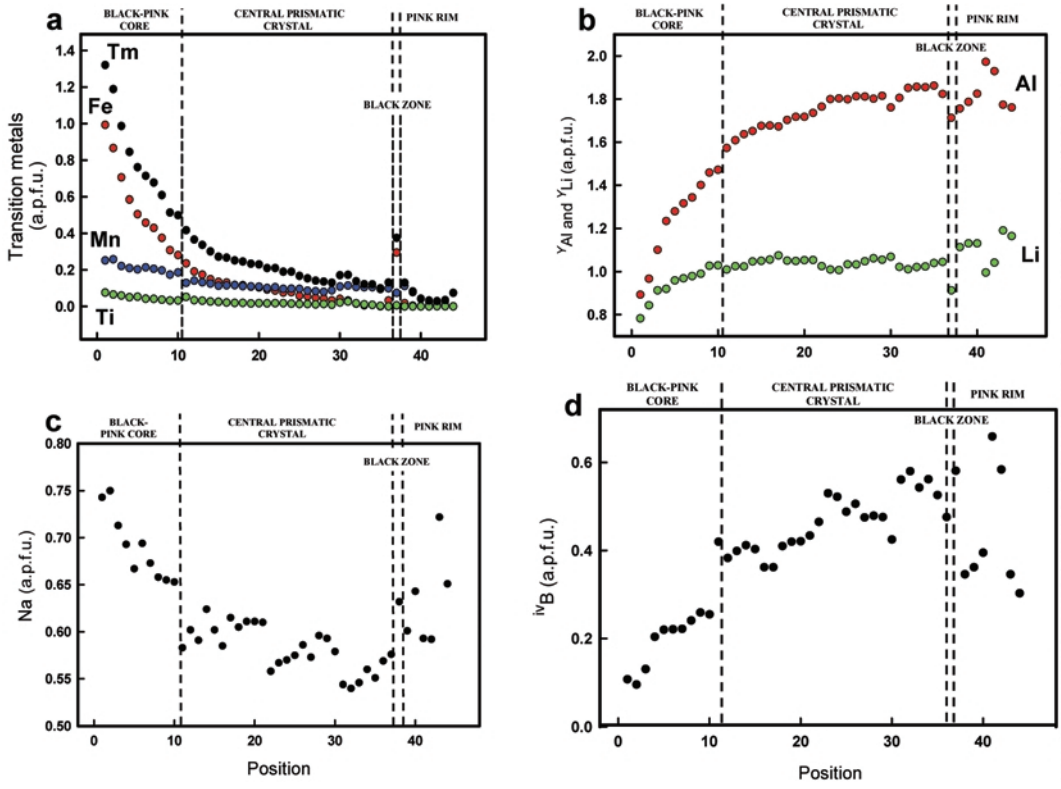

FIG. 5. Variation in chemical composition of SHM as a function of position along traverse 1, Fig. 4: (*a*) Total transition metals (Tm) – black; Fe – red; Mn – blue; Ti – green; (*b*) ^{Y}Al (red) and Li (green); (*c*) ^{iv}B; (*d*) Na.

in the first part of the crystal are summarized as follows:

(1) $^{Y}\text{Li} + {}^{Y}\text{Al} \rightarrow {}^{Y}\text{Fe}^{*} + {}^{Y}\text{Fe}^{*}$ 0.06 a.p.f.u.
(5) $\square + {}^{Y}\text{Al} + \text{Si} \rightarrow \text{Ca} + {}^{Y}\text{Fe}^{*} + {}^{T}\text{B}$ 0.06 a.p.f.u.

At the boundary shown by the dashed line in Fig. 6*b*, there is a break in each constituent, but Li and B are particularly important as their variation changes sign, denoting a significant change in the substitutions as this point. As the variations in Li

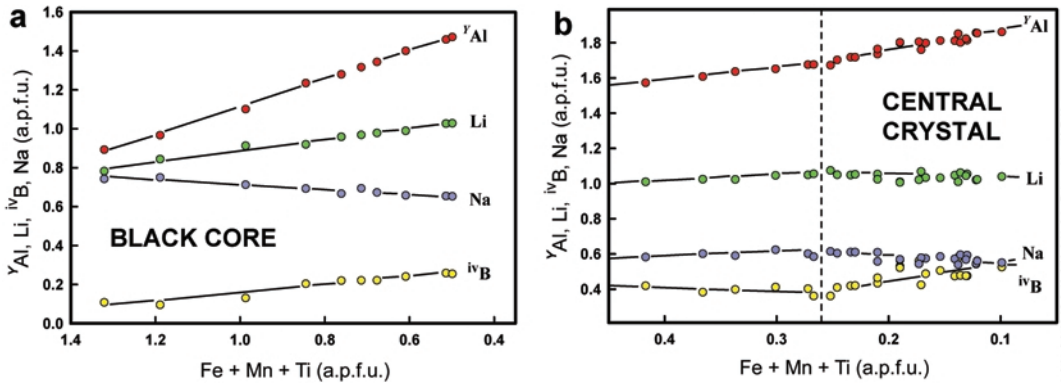

FIG. 6. Variation in chemical composition of SHM as a function of total transition-metals along traverse 1, Fig. 4: (*a*) black core; (*b*) central prismatic crystal.

and ^{Y}Al are no longer sympathetic, substitution 1 is no longer active. ^{iv}B begins to increase again *via* substitution 2, and the remaining changes are accounted for by substitution 6:

(2) $^{T}B + {}^{Y}Al \rightarrow Si + {}^{Y}Fe^{*}$ 0.12 a.p.f.u.
(6) $2^{X}\square + {}^{Y}Al \rightarrow Na_2 + Li$ 0.02 a.p.f.u.

At the black zone, there is a sudden increase in Fe and decrease in Mn (Fig. 5*a*) that reverses on the other size of the black zone. Both Li and Al drop sharply at the black zone (Fig. 5), indicating that this zone corresponds to sudden activity of substitution 1.

In the outer pink zone, ^{iv}B decreases sharply from ~0.80 to >0.30 a.p.f.u. (Traverse 3, Figs 4, 7*a*), accompanied by significant increases in Li and Na, and decreases in ^{Y}Al and Fe*. Figure 7*b* shows the chemical variations in the pink zone, not as a function of Fe* (as this is now extremely low), but of ^{iv}B. Again, there is a very coherent variation in chemical constituents. Following the same procedure as above, we may identify the substitutions operative as (7) and (8):

(7) $Li + Si \rightarrow Fe^{*} + {}^{T}B$ 0.20 a.p.f.u.
(8) $Li + Si_2 \rightarrow {}^{Y}Al + {}^{T}B_2$ 0.16 a.p.f.u.

Kalt *et al.*, 2001 proposed substitution 2 for the incorporation of ^{iv}B into olenite-schorl tourmalines, and this is also a major substitution accounting for the variation in ^{iv}B in SHM, although it is not the only major substitution that involves ^{T}B in SHM.

In order to assess the relative timing of the growth of the different zones of the mushroom, we also examined the variation in composition across crystal SHM (Traverse 2, Figs 4, 8). There are four distinct zones that correspond to the texturally different regions of the crystal. In the central prismatic zone, the transition metals decrease slightly towards the edge (Fig. 8*a*), Al increases slightly and Li decreases slightly (Fig. 8*b*), ^{iv}B increases slightly (Fig. 8*c*) and the *X*-site constituents are fairly constant. At the boundary with the region where there is the transition from a coherent single crystal to acicular crystals, there is a sharp increase in all of the transition metals (Fig. 8*a*) and a drop in ^{Y}Al (Fig. 8*b*). All other constituents show no discontinuity at this boundary, although their variation within the transition region is much more irregular than in the central prismatic crystal. At the boundary between the transition region and the acicular crystals, again there is an increase in the transition metals (Fig. 8*a*), small discontinuities in ^{Y}Al and Li (Fig. 8*b*), a very large discontinuity in ^{iv}B (Fig. 8*c*), and discontinuities in Na and Ca but not in $^{X}\square$ (Fig. 8*d*). In addition, Fig. 8 also shows a specific point within the acicular region (marked A in Fig. 8) that shows a strong compositional difference with the adjacent regions.

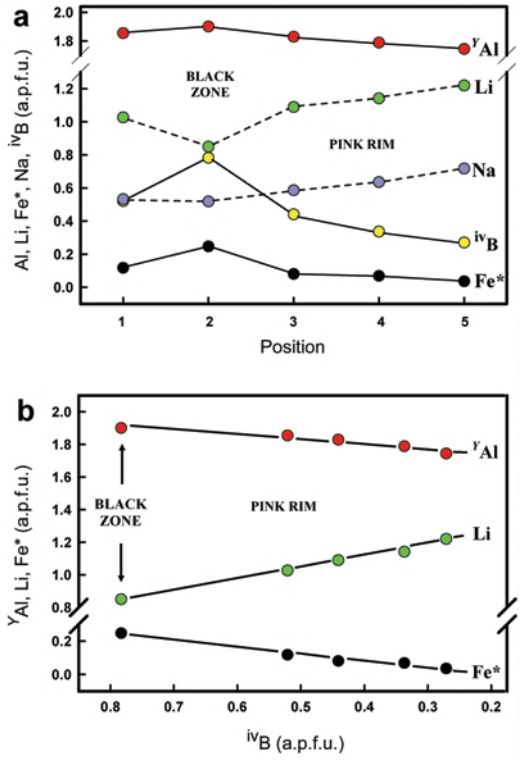

FIG. 7. Variation in chemical composition of SHM along traverse 3, Fig. 4: (*a*) composition as a function of position; (*b*) ^{Y}Al, Li and Fe* (= Fe + Mn + Ti) as a function of ^{iv}B content.

The variation in composition as a function of transition-metal content along the same section is shown in Fig. 9. The data for the central prismatic crystal and the acicular region show continuous linear variations in ^{Y}Al, Li, ^{iv}B and Na that are similar to the variations shown in Fig. 6*b*, whereas the transition zone (Fig. 9) shows more extreme variations with ^{iv}B being rather irregular.

Growth of mushroom tourmaline

Both texturally and compositionally, we have distinguished five different parts of the mushroom tourmaline: (1) the black-grey core; (2) the central prismatic crystal; (3) the zone of transition from

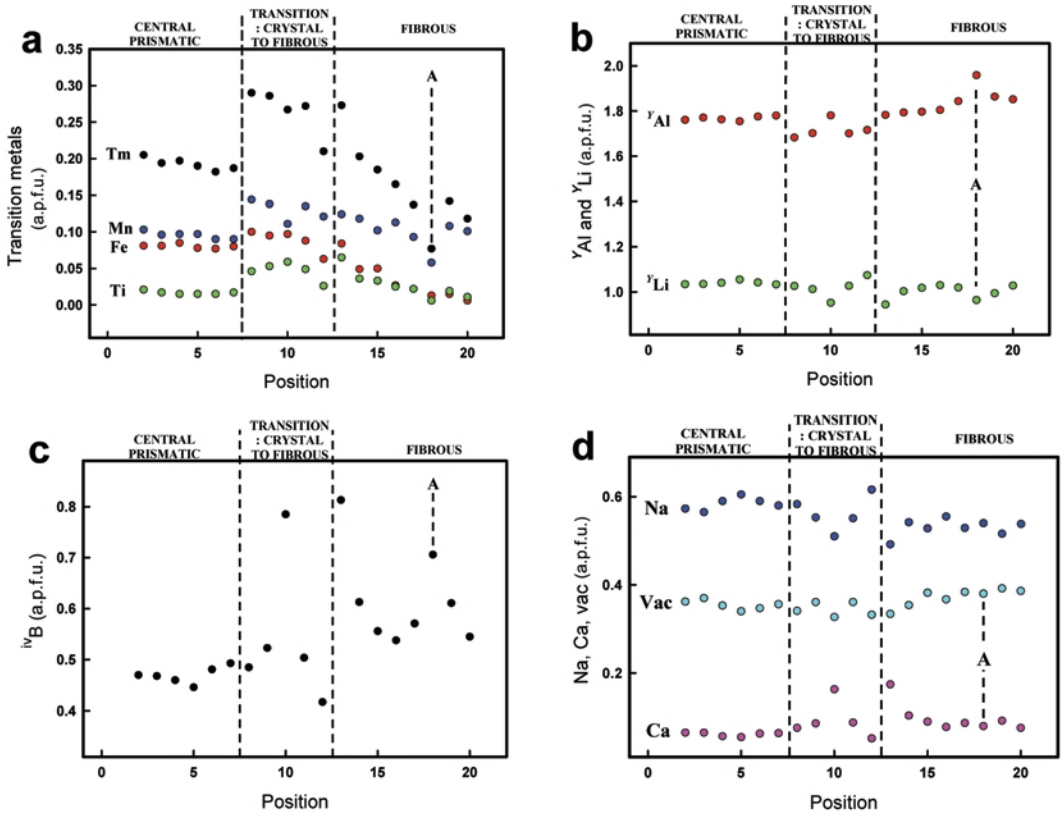

FIG. 8. Variation in chemical composition of SHM as a function of position along traverse 2, Fig. 4: (*a*) transition metals; (*b*) ^{Y}Al and Li; (*c*) ^{iv}B; (d) Na, Ca and $^{X}\square$. Line A is referred to in the text.

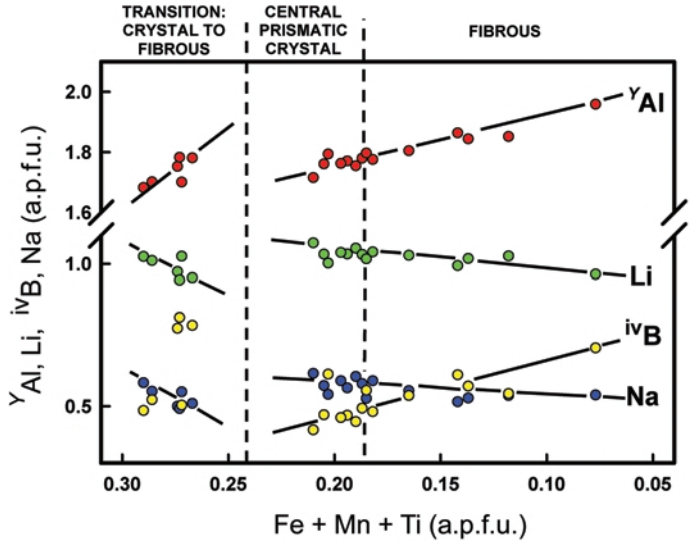

FIG. 9. Variation in chemical composition of SHM as a function of total transition-metals along traverse 2, Fig. 4.

single crystal to acicular crystals; (4) the acicular zone, which includes the thin black zone towards the edge of the mushroom. On the basis of the textural and compositional data, the following growth model for the mushroom tourmaline may be developed.

Phase I

Growth began with nucleation and initial growth of a single crystal, and this phase progressed to produce a stout (probably euhedral) crystal that now forms the core of the mushroom (Figs 1, 2*a*). Crystallization rapidly depleted the environment in transition metals (Fig. 5*a*) and Na, with a concomitant increase in both ^{Y}Al and Li (Fig. 5*b*) and ^{iv}B (Fig. 5*d*).

Phase II

The central prismatic crystal began to grow from the black core (Fig. 5*b*), accompanied by smaller prismatic crystals to each side that do not develop to the same extent (Figs 2*b*, 3). There are marked discontinuities in Na (Fig. 5*c*), ^{iv}B (Fig. 5*d*), ^{Y}Al and Li (Fig. 5*b*) and small discontinuities in Mn and Ti but not Fe (Fig. 5*a*) where this type of growth began. The central prismatic crystal continued to grow with further decrease in transition metals and Na, and increase in ^{Y}Al, Li and ^{iv}B.

Phase III

Very acicular crystals began to grow from the end of the central prismatic crystal further from the core (Fig. 10*c*), with similar growth from the smaller subsidiary crystals to either side of the main prismatic crystal. At this stage, there are significant discontinuities in the composition of the crystallizing tourmaline, with small increases in transition metals (Fig. 5*a*), a drop in Na (Fig. 5*c*), and decreases in ^{Y}Al, Li and ^{iv}B (Fig. 5*b*,*d*). The narrow black band that occurs towards the edge of the mushroom provides a constraint on growth of the acicular tourmaline: compositional changes indicate that growth of acicular crystals began contemporaneously at all places in the mushroom. As a result, growth must have been much more rapid in the peripheral parts of the mushroom than at the end of the central

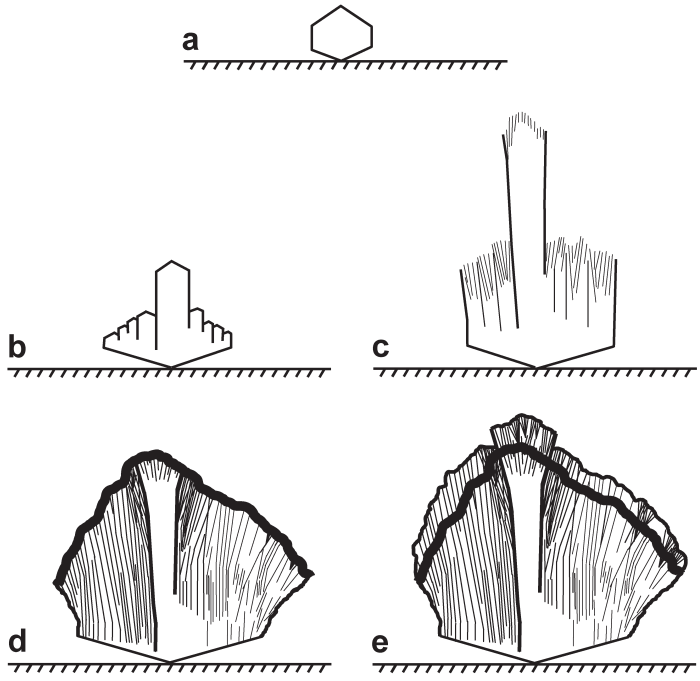

FIG. 10. Model of the growth process in mushroom tourmaline: (*a*) nucleation and growth of the single-crystal black core; (*b*) growth of central prismatic crystal; (*c*) initiation of fibre growth; (*d*) growth of black band during fibre growth; (*e*) growth of the final dense intergrowth of fibres at the surface.

prismatic crystal. This is in accord with the strong compositional discontinuity between the central crystal and the adjacent transition regions in traverse 2 (Fig. 8). The acicular crystals tend to curve away from the central axis of the mushroom (Fig. 3*c*), and there may be nucleation and growth of new crystals on the sides of pre-existing crystals.

Phase IV

The black band (Figs 1, 2) is characterized by a strong increase in transition metals (Fig. 5*a*) and Na (Fig. 5*c*) and a decrease in the other constituents. This presumably reflects a pulse of fluid rich in transition metals. Unfortunately, we have no information on the local environment of the mushroom tourmalines within their parent pegmatites. However, the unusual habit suggests growth within a miarolitic cavity in which the tourmaline could grow unimpeded by other minerals. This being the case, the black band may mark cavity rupture, with a resulting drop in P_{H_2O}. The spike in transition metals may result from the sudden change in P_{H_2O} or an influx of fluid of different composition. Certainly, the sharp increase in Na and Li and the decrease in ^{iv}B and Al at and outside the black band (Figs 5, 7) suggest influx of a more alkali-rich fluid.

Phase V

During this final stage of growth, acicular crystals continued to develop, forming dense and elaborate intergrowths (Fig. 3*d*).

Growth conditions

The general transition from Fe-bearing to Fe-absent tourmaline along the growth profile of the sample (with exception of the pink region) is consistent with a typical evolutionary trend of tourmaline composition in granites and pegmatites during fractionation (e.g. Jolliff *et al.*, 1986). The stability field for elbaite spans large ranges in pressure (100–400 MPa) and temperature (300–750ºC; Vorbach, 1989), hence it is difficult to bracket the *P-T* conditions of the mushroom growth. London (1986) suggested that the development of tourmaline-rich pockets in rare-element pegmatites occurs in the range 425–475ºC and 240–280 MPa. However, this temperature estimate is greater than that suggested by the fluid-inclusion work of Zaw (1998) that puts the formation temperature of some pegmatites in Myanmar between 210 and 410ºC.

The textural and optical continuity from the base of the mushroom to the tips of the pink fibres (Fig. 2) suggests that there was no dissolution of previously precipitated tourmaline. The nucleation of secondary crystals on the sides of those already present is in accord with the solution being consistently supersaturated with respect to the tourmaline being precipitated. The overall compositional change from core to rim (Figs 5, 8) is consistent with depletion of the nascent fluid in transition metals. However, there are significant abrupt compositional discontinuities at positions 11, 21 and 30 (Figs 5, 6) at which the substitution mechanisms change. Further, the discontinuities between positions 21 and 30 are more pronounced in some constituents (e.g. Na and B) than in others (e.g. Li and Al). Hence it is difficult to state whether or not these discontinuities result from the influx of new magmatic (or hydrothermal) fluids, or to the saturation and subsequent crystallization of other minerals proximal to the growing mushroom, which would selectively affect only certain elements. The major compositional discontinuity at position 37 (Figs 4, 5) strongly suggests pocket rupture, with the introduction of a more mafic fluid, probably due to influxing of Fe* from fluid interaction with mafic wallrocks (e.g. London and Manning, 1985; Foord *et al.*, 1986; London, 1999).

Summary

(1) Mushroom tourmaline SHM consists of a black-to-grey single-crystal core from which a single prismatic crystal protrudes to reach the edge of the mushroom. The rest of the mushroom consists of sub-parallel colourless-to-white acicular crystals that diverge toward the edge off the mushroom, becoming pale pink outside a narrow black zone just inside the edge.

(2) There are eight distinct substitution mechanisms involved in the chemical variation within the mushroom tourmaline, which varies in composition from ~$Na_{0.75}Ca_{0.05}(Li_{0.80}Al_{0.70}Fe_{1.10}Mn_{0.30}Ti_{0.10})Al_6Si_6(BO_3)_3O_{18}(OH)_3(OH,F)$ at the base to ~$Na_{0.60}Ca_{0.06}(Li_{1.00}Al_{1.98}Fe_{0.02})Al_6(Si_{5.35}B_{0.65})(BO_3)_3O_{18}(OH)_3(OH,F)$ close to the rim. Of interest are the three substitutions that involve variation in ^{T}B:

$$^{T}B + {}^{Y}Al \rightarrow Si + {}^{Y}Fe^{*}, \quad (2)$$

$$Li + Si \rightarrow Fe^{*} + {}^{T}B \text{ and} \quad (7)$$

$$Li + Si_2 \rightarrow {}^{Y}Al + {}^{T}B_2 \quad (8)$$

(3) At the boundaries of the different zones of the mushroom, there are distinct breaks in

composition, and new substitution mechanisms become operative.

(4) Growth of a single core crystal and major depletion of transition metals in the immediate environment was followed by growth of a long prismatic crystal accompanied by much shorter prismatic crystals to each side. Acicular crystals began to grow from the end of the central prismatic crystal further from the core, with similar growth from the smaller subsidiary crystals, again with a significant compositional discontinuity. Extensive growth of acicular tourmaline was interrupted by a sudden increase in transition metals and the formation of a thin black band close to the edge of the tourmaline. Acicular crystals continued to grow as a dense and elaborate intergrowth that forms the outer surface of the mushroom.

(5) The general transition from Fe-bearing to Fe-absent tourmaline along the growth profile of the sample (with exception of the pink region) is consistent with a typical evolutionary trend of tourmaline composition in granites and pegmatites during fractionation.

(6) Changes in texture of the tourmaline are accompanied by compositional discontinuities in which the variation of ^{iv}B in particular is of major quantitative significance.

(7) In the absence of detailed field relations, it is difficult to state whether or not these compositional discontinuities result from the influx of new fluids, or to the saturation and subsequent crystallization of other minerals proximal to the growing mushroom. However, the major compositional discontinuity at the black rim of the mushroom strongly suggests pocket rupture, with the introduction of a more mafic fluid, probably due to influxing of Fe* from fluid interaction with mafic wallrocks.

Acknowledgements

We thank Barbara Dutrow and George Harlow for their significant comments on this manuscript. This work was funded by University of Manitoba Graduate Fellowships AJL, SH and VKM, an NSERC PGS-D to AJL, by a Canada Research Chair in Crystallography and Mineralogy, and by Major Facilities Access grants to FCH, and by Research Tools and Equipment, and Discovery Grants to FCH and SK from the Natural Sciences and Engineering Research Council of Canada, and by Canada Foundation for Innovation Grants to FCH and SK.

References

Bloodaxe, E.S., Hughes, J.M., Dyar, M.D., Grew, E.S. and Guidotti, C.V. (1999) Linking structure and chemistry in the schorl–dravite series. *American Mineralogist*, **84**, 922–928.

Cempírek, J., Novak, M., Ertl, A., Hughes, J.M., Rossman, G.R. and Dyar, M.D. (2006) Fe-bearing olenite with tetrahedrally coordinated Al from an abyssal pegmatite at Kutna Hora, Czech Republic: structure, crystal chemistry, optical and XANES spectra. *The Canadian Mineralogist*, **44**, 23–30.

Dutrow, B.L. and Henry, D.J. (2000) Complexly zoned fibrous tourmaline, Cruzeiro Mine, Minas Gerais, Brazil: a record of evolving magmatic and hydrothermal fluids. *The Canadian Mineralogist*, **38**, 131–143.

Ertl, A. and Hughes, J.M. (2002) The crystal structure of an aluminum-rich schorl overgrown by boron-rich olenite from Koralpe, Styria, Austria. *Mineralogy and Petrology*, **75**, 69–78.

Ertl, A., Pertlik, F. and Berhardt, H.-J. (1997) Investigations on olenite with excess boron from the Koralpe, Styria, Austria. *Anzeiger*, **134**, 3–10.

Ertl, A., Hughes, J.M., Brandstätter, F., Dyar, M.D. and Prasad, P.S.R. (2003) Disordered Mg-bearing olenite from a granitic pegmatite from Goslarn, Austria: A chemical, structural and infrared spectroscopic study. *The Canadian Mineralogist*, **41**, 1363–1370.

Ertl, A., Rossman, G.R., Hughes, J.M., Prowatke, S. and Ludwig, T. (2005) Mn-bearing "oxy-rossmanite" with tetrahedrally coordinated Al and B from Austria: structure, chemistry, and infrared and optical spectroscopy. *American Mineralogist*, **90**, 481–487.

Ertl, A., Hughes, J.M., Prowatke, S., Ludwig, T., Prasad, P.S.R., Brandstatter, F., Korner, W., Schuster, R., Pertlik, F. and Marschall, H. (2006) Tetrahedrally coordinated boron in tourmalines from the liddicoatite-elbaite series from Madagascar: structure, chemistry, and infrared spectroscopic studies. *American Mineralogist*, **91**, 1847–1856.

Ertl, A., Hughes, J.M., Prowatke, S., Ludwig, T., Brandstatter, F., Korner, W. and Dyar, M.D. (2007) Tetrahedrally coordinated boron in Li-bearing olenite from 'Mushroom' tourmaline from Momeik, Myanmar. *The Canadian Mineralogist*, **45**, 891–899.

Federico, M., Andreozzi, G.B., Lucchesi, S. and Graziani, G. (1998) Compositional variation of tourmaline in the granitic pegmatite dykes of the Cruziero mine, Minas Gerais, Brazil. *The Canadian Mineralogist*, **36**, 415–431.

Foord, E.E., Starkey, H.C. and Taggert, J.E. Jr. (1986) Mineralogy and paragenesis of 'pocket' clays and associated minerals in complex granitic pegmatites, San Diego County, California. *American*

Mineralogist, **71**, 428–439.

Hughes, J.M., Ertl, A., Dyar, M.D., Grew, E.S., Shearer, C.K., Yates, M.G. and Guidotti, C.V. (2000) Tetrahedrally coordinated boron in tourmaline: boron-rich olenite from Stoffhutte, Koralpe, Austria. *The Canadian Mineralogist*, **38**, 861–868.

Hughes, K.-A., Hughes, J.M. and Dyar, M.D. (2001) Chemical and structural evidence for $^{[4]}B \Leftrightarrow {}^{[4]}Si$ substitution in natural tourmalines. *European Journal of Mineralogy*, **13**, 743–747.

Hughes, J.M., Ertl, A., Dyar, M.D., Grew, E.S., Wieden-Beck, M. and Brandstatter, F. (2004) Structural and chemical response to varying $^{[4]}B$ content in zoned Fe-bearing olenite from Koralpe, Austria. *American Mineralogist*, **89**, 447–454.

Jolliff, B.L., Papike, J.J. and Shearer, C.K. (1986) Tourmaline as a recorder of pegmatite evolution: Bob Ingersoll pegmatite, Black Hills, South Dakota. *American Mineralogist*, **71**, 472–500.

Kalt, A., Schreyer, W., Ludwig, T., Prowatke, S., Bernhardt, H.-J. and Ertl, A. (2001) Complete solid solution between magnesian schorl and lithian excess-boron olenite in a pegmatite from the Koralpe (eastern Alps, Austria). *European Journal of Mineralogy*, **13**, 1191–1205.

London, D. (1986) Formation of tourmaline-rich gem pockets in miarolitic pegmatites. *American Mineralogist*, **71**, 396–405.

London, D. (1999) Stability of tourmaline in peraluminous granite systems: the boron cycle from anatexis to hydrothermal aureoles. *European Journal of Mineralogy*, **11**, 253–262.

London, D. and Manning, D.A.C. (1995) Chemical variation and significance of tourmaline from Southwest England. *Economic Geology*, **90**, 495–519.

Lussier, A.J., Aguiar, P.M., Michaelis, V.K., Kroeker, S., Herwig, S., Abdu, Y. and Hawthorne, F.C. (2008) Mushroom elbaite from the Kat Chay mine, Momeik, near Mogok, Myanmar: I. Crystal chemistry by SREF, EMPA, MAS NMR and Mössbauer spectroscopy. *Mineralogical Magazine*, **72**, 747–761.

Lussier, A.J., Aguiar, P., Michaelis, V., Kroeker, S. and Hawthorne, F.C. (2009) The occurrence of tetrahedrally coordinated Al and B in tourmaline: A ^{11}B and ^{27}Al MAS NMR study. *American Mineralogist*, (in press).

Macdonald, D.J. and Hawthorne, F.C. (1995) The crystal chemistry of Si-Al substitution in tourmaline. *The Canadian Mineralogist*, **33**, 849–858.

Marler, B. and Ertl, A. (2002) Nuclear magnetic resonance and infrared spectroscopic study of excess-boron olenite from Koralpe, Styria, Austria. *American Mineralogist*, **87**, 364–367.

Marler, B., Borowski, M., Wodara, U. and Schreyer, W. (2002) Synthetic tourmaline (olenite) with excess boron replacing silicon in the tetrahedral site: II. Structure analysis. *European Journal of Mineralogy*, **14**, 763–771.

Prowatke, S., Ertl, A. and Hughes, J.M. (2003) Tetrahedrally-coordinated Al in Mn-rich, Li- and Fe-bearing olenite from Eibenstein an der Thaya, Lower Austria: A chemical and structural investigation. *Neues Jahrbuch für Mineralogie, Monatshefte*, 2003, 385–395.

Schreyer, W., Wodara, U., Marler, B., van Aken, P.A., Seifert, F. and Robert, J.-L. (2000) Synthetic tourmaline (olenite) with excess boron replacing silicon in the tetrahedral site: I. Synthesis conditions, chemical and spectroscopic evidence. *European Journal of Mineralogy*, **12**, 529–541.

Schreyer, W., Hughes, J.M., Bernhardt, H.-J., Kalt, A., Prowatke, S. and Ertl, A. (2002) Reexamination of olenite from the type locality: detection of boron in tetrahedral coordination. *European Journal of Mineralogy*, **14**, 935–942.

Selway, J.B., Novàk, M., Černý, P. and Hawthorne, F.C. (1999) Compositional evolution of tourmaline in lepidolite-subtype pegmatites. *European Journal of Mineralogy*, **11**, 569–584.

Selway, J.B., Černý, P., Hawthorne, F.C. and Novák, M. (2000) The Tanco pegmatite at Bernic Lake, Manitoba. XIV. Internal tourmaline. *The Canadian Mineralogist*, **38**, 877–891.

Selway, J.B., Smeds, S.-A., Černý, P. and Hawthorne, F.C. (2002) Compositional evolution of tourmaline in the petalite-subtype Nyköpingsgruvan pegmatites, Utö, Stockholm Archipelago, Sweden. *GFF*, **124**, 93–102.

Tagg, S.L., Cho, H., Dyar, M.D. and Grew, E.S. (1999) Tetrahedral boron in naturally occurring tourmaline. *American Mineralogist*, **84**, 1451–1455.

Vorbach, A. (1989) Experimental examinations on the stability of synthetic tourmalines in temperatures from 250ºC to 750ºC and pressures up to 4 kb. *Neues Jahrbuch für Mineralogie Abhandlung*, **161**, 69–83.

Zaw, K. (1998) Geological evolution of selected granitic pegmatites in Myanmar (Burma): constraints from regional setting, lithology, and fluid-inclusion studies. *International Geology Review*, **40**, 647–662.